Applied Catalysis B: Environmental 303 (2022) 120898

Contents lists available at ScienceDirect

Applied Catalysis B: Environmental

journal homepage: www.elsevier.com/locate/apcatb

Measurement and Modeling of the effects of exhaust composition and hydrothermal aging on the ammonia storage capacity of a commercial Cu-SSZ-13 catalyst

Austin Ladshaw, Josh Pihl *

Oak Ridge National Laboratory, USA

ARTICLE INFO

Keywords:
Ammonia storage
Selective catalytic reduction
Copper chabazite
Aging
Modeling

ABSTRACT

Copper exchanged chabazites are among the state-of-the-art catalyst materials being studied for selective catalytic reduction of NOx, however, there is still a need to understand how these materials store ammonia after aging. In this work, studies are performed to assess the ammonia storage capacity of Cu-SSZ-13 as a function of concentration, temperature, and extent of hydrothermal aging. Ammonia binds at three difference sites: (i) a Cu site bound at 1 framework Al (Z_1Cu site), (ii) a Cu site bound at 2 framework Al (Z_2Cu site), and (iii) a Brønsted acid site (ZH site). Results show that a 3-site model can accurately capture ammonia storage across all conditions. Impacts for hydrothermal aging are considered via 3 aging reactions that change the site densities of each identified adsorption site. Model assessment shows that during aging there is a significant loss in Brønsted acid sites.

Symbols.

Latin

A_i	Pre-exponential factor for forward or reverse rate constants (L/mol/min).
$C_{b,i}$	Gas-phase concentrations of adsorbate i in the bulk phase of the monolith (mol/L).
C_i	Gas-phase concentrations of adsorbate i in the pore-space of Cu-SSZ-13 (mol/L).
E_i	Activation energy for forward or reverse rate constants (J/mol).
G_a	Surface area to volume ratio for the washcoat layer of the catalyst (m^{-1}).
K_i	Binding affinity or equilibrium constant for site i (L/mol).
k_i	Forward rate constant for aging reaction i.
k_{-i}	Reverse rate constant for aging reaction i.
$k_{f,i}$	Forward rate constant for the i^{th} adsorption reaction (L/mol/min).
$k_{r,i}$	Reverse rate constant for the i^{th} adsorption reaction (min^{-1}).
$k_{m,i}$	Effective mass-transfer rate from bulk to pore-space (m/min).
q_i	Molar concentration of NH_3 adsorbed to site i (mol/L).
q_T	Total molar concentration of all NH_3 adsorbed (mol/L).
R	Gas law constant (J/K/mol).
r_i	Overall rate of adsorption for i^{th} adsorption reaction (mol/L/min).
S_k	Surface concentration of a specific adsorption site at a point in time (mol/L).
T	Isothermal gas temperature (K).
u_i	Molar stoichiometry for additional adsorbed NH_3 to the i^{th} adsorption site.
w_i	Site density or total availability for site i (mol/L).

Greek

ΔG_r	Gibb's free energy of reaction (kJ/mol).
ΔH_i	Adsorption enthalpy for reaction i (J/mol).
ΔS_i	Adsorption entropy for reaction i (J/K/mol).
α	Ratio of Z_2Cu occupied by only a single NH_3 in presence of H_2O.
β	Ratio of Z_2Cu occupied by 2 NH_3 in the presence of H_2O.
γ	Ratio of Z_2Cu occupied by H_2O in the absence of NH_3.
ε_b	Bulk monolith void space per total volume.
ε_w	Volume of washcoat pores per volume of washcoat.

Other

$[i]_t$	Surface concentration of i after aging time t (mol/L).

* Correspondence to: National Transportation Research Center, Energy Science & Technology Directorate, Oak Ridge National Laboratory, 1 Bethel Valley Road, Oak Ridge, TN 37830

E-mail address: pihlja@ornl.gov (J. Pihl).

https://doi.org/10.1016/j.apcatb.2021.120898
Received 22 July 2021; Received in revised form 6 October 2021; Accepted 2 November 2021
Available online 6 November 2021

$[i]_o$ Initial surface concentration of i before aging (mol/L).

Manuscript.

1. Introduction

Vehicle aftertreatment systems, such as Selective Catalytic Reduction (SCR) catalysts, are integral components of the exhaust systems necessary to reduce tailpipe pollutants including oxides of nitrogen (NOx). As engine technologies evolve over time, so must the catalyst technology in order to keep up with the changing compositions and temperatures of the engine exhaust, as well as changes in emission standards.[1,2] In recent years, the usage of commercial copper exchanged zeolites, and especially chabazites (Cu-CHA) such as Cu-SSZ-13 and Cu-SAPO-34, for selective catalytic reduction (SCR) of NOx has been the subject of numerous studies.[3–11] These commercial materials have quickly become the primary focus for SCR research due to their efficiency at low temperature NOx conversion [12–15], along with improved performance and hydrothermal aging resistance compared to prior materials. [3,4,16–21].

While much prior research has been focused on the reaction mechanisms that drive the NOx conversion reactions within Cu-CHAs, industry has identified that there is still a need for a fundamental understanding of the mechanisms by which ammonia (NH_3) is stored in the catalyst and how that storage can be impacted by exhaust operating conditions and hydrothermal aging.[22] There is a connection between NH_3 storage and SCR performance, thus any environmental or operational condition that impacts that storage must be quantified and modeled accurately so that exhaust systems can be designed to meet long-term NOx reduction and NH_3 storage needs.[2,22,23] This is especially critical considering the proposed durability requirements for heavy duty emissions control systems under consideration by the California Air Resources Board (CARB), which may increase the useful life demands of the emission control system from 435,000 miles to 800,000 miles.[24] One of the most common metrics for quantifying NH_3 storage, as well as the impact of hydrothermal aging, on Cu-CHAs is to measure NH_3 temperature programmed desorption (TPD) curves.[19, 21,25–29].

Numerous studies of Cu-SSZ-13, as well as other Cu-CHAs, which measured NH_3-TPDs all show very similar characteristic curves that involve a low temperature NH_3 desorption peak followed by a secondary peak at higher temperature.[5–9,14,18,19,21,25–29] The general consensus among researchers is that the low temperature peak corresponds to NH_3 stored on the Cu sites of Cu-SSZ-13, while the high temperature peak corresponds to NH_3 stored on the Brønsted acid sites, although some recent works suggest that each peak may be a mixture of Cu sites and Brønsted sites [30,31]. During the reduction of NOx, the NH_3 bound to Cu sites are considered actively involved with the catalytic reaction. As the Cu-bound NH_3 is utilized, NH_3 from the Brønsted sites, which are considered inactive in the NOx reaction, can migrate to the Cu sites.[12,14,23,27,32] Thus, the availability of Brønsted acid sites likely plays some role in the efficiency of the SCR NOx conversion reactions.

Some studies have also utilized TPD curves to assess the impact of hydrothermal aging on NH_3 storage.[5,19,21,25,26] For instance, Luo et al. [25] develop a simple metric to quantify aging based on the ratio of the area under the low temperature peak of the TPD to the area under the high temperature peak of the TPD at different aging conditions. The work by Luo et al. [25] demonstrated that during hydrothermal aging there is a loss of NH_3 storage capacity on Brønsted sites accompanied by a gain in NH_3 storage capacity on Cu sites. Thus, there must be some mechanism by which Brønsted acid sites can be lost as active Cu sites are formed. Those newly formed Cu sites can store NH_3 and may also improve the NOx conversion efficiency since they are considered active in the reduction reaction. This phenomenon is qualitatively logical, as the calcination process used to prepare Cu-SSZ-13 materials prior to use is essentially a form of mild hydrothermal aging.[18] However, losing Brønsted sites means a loss in high temperature ammonia storage, which may have a competing negative impact on NOx conversion, especially at higher temperatures. Thus, there is likely some balance needed between active Cu sites for direct NOx conversion and Brønsted sites as reservoirs for ammonia storage.

Taking these theoretical and observational considerations into account, the goal of this work is to develop models to accurately quantify the storage of Cu-SSZ-13 under a variety of NH_3 concentrations, gas temperatures, water vapor concentrations, and hydrothermal aging times. While some models for ammonia storage on Cu-SSZ-13 are already available in the literature [33–35], those existing models either: (i) do not account for hydrothermal aging, (ii) are only calibrated to a narrow concentration range of ammonia, or (iii) do not make clear distinctions between Cu sites and Brønsted sites. Thus, there is still a need to develop a more unified model approach for ammonia storage on Cu-SSZ-13. Based on the above literature review, the models developed in this work must be able to distinguish between NH_3 storage on Cu sites and Brønsted sites and include aging mechanisms to account for the transformation of Brønsted sites into Cu sites, as well as the potential to form copper oxide clusters (CuO).[6,18] Furthermore, the model must be consistent with phenomena observed in TPDs, such as the temperature separation between Brønsted-NH_3 and Cu-NH_3.[25–29,32].

To supplement the modeling efforts, a significant amount of NH_3 storage data on a commercial Cu-SSZ-13 catalyst has been collected to calibrate the model and produce the necessary model parameters. Isothermal storage capacities for NH_3 are collected at gas concentrations ranging from 12.5 to 1000 ppmv NH_3 for temperatures between 150 and 350 °C. Those isothermal capacities are performed for a "de-greened" Cu-SSZ-13 material, then repeated for Cu-SSZ-13 that was aged at 800 °C for 2, 4, 8, and 16 h. To assess the impact of water vapor on NH_3 storage, additional experiments were conducted by keeping the NH_3 gas concentration at 400 ppmv and changing the water vapor content of the gas from 3% to 11%.

The NH_3 storage model was developed based on the hypothesis that the changes in NH_3 storage with aging could be captured by changing only the NH_3 storage site densities. To confirm this hypothesis, the NH_3 storage model must be able to describe all experimental storage results with a single common set of thermodynamic parameters (adsorption enthalpies and entropies).

2. Experimental Methods

2.1. Copper Chabazite Material

The catalyst material used in this study was a commercial Cu-SSZ-13 monolith used in General Motors (GM) diesel pick-up trucks. A 2 cm diameter by 5 cm length core sample was cut from the full-size SCR part for use in the synthetic exhaust flow reactor experiments. Elemental analysis is provided in Table 1 below. The sample had a Si/Al molar ratio of about 15 and a Cu/Al molar ratio of about 0.42. The Zr in the catalyst is assumed to be functionally inert with respect to ammonia binding. Prior to use, the sample was "de-greened" at 700 °C for 4 h in 10% O_2 and 10% H_2O. For the subsequent aging studies, the core was hydrothermally aged for 2, 4, 8, or 16 h at 800 °C in 10% O_2 and 10% H_2O.

Table 1
Summary of the elemental analysis of the commercial Cu-SSZ-13 catalyst used in this study.

Element	Wt. Fraction
Cu	2.1%
Al	2.1%
Si	33%
Zr	3.0%

2.2. 2.2. Flow Reactor

Experiments in this work were performed on an automated synthetic exhaust flow reactor described elsewhere [36]. Briefly, the flow reactor used mass flow controllers, an HPLC pump, and a custom water vaporizer to create relevant but carefully controlled synthetic exhaust gas compositions. The catalyst core sample was placed inside a tube furnace to control the temperature, and five thermocouples (radial center and inlet, radial center and axial midpoint, radial edge and axial midpoint, radial center and outlet, radial edge and outlet) were used to confirm that the catalyst core was maintained at isothermal ($\pm$ 2 °C) conditions. The entire flow reactor system was controlled with a custom LabVIEW interface. Inlet and outlet gas compositions were measured using a Fourier Transform Infrared (FTIR) Spectrometer (MKS Instruments). All experimental campaigns and aging protocols were done in line such that the core sample never needed to be removed from the reactor setup.

2.3. NH_3 Isotherm Studies

NH_3 storage on Cu-SSZ-13 is evaluated by stepwise desorption experiments at a series of isothermal temperatures from 150 °C to 350 °C. For each temperature, the catalyst is first exposed to a gas flow containing 1000 ppmv of NH_3 and 5% H_2O until the catalyst is saturated with NH_3. Then, the concentration of NH_3 is stepped down, allowing the stored NH_3 to desorb until a new equilibrium point is reached. This step is repeated for additional steps down in NH_3 concentration to a minimum NH_3 of 12.5 ppmv. During all experiments, the total gas flow rate is held constant at a gas hourly space velocity (GHSV) of 30,000 h^{-1} based on flows at 1 atm and 0 °C and the total volume of the catalyst core sample. The adsorbed amounts of NH_3 are calculated by integrating the difference between the inlet and outlet concentrations over time. After the final equilibrium point at 12.5 ppmv NH_3 is evaluated, the NH_3 flow is shut off and the temperature in the system is raised linearly to around 550 °C to desorb any remaining NH_3 on the catalyst and produce a series of TPD curves.

2.4. Impact of Water Vapor

Assessment of the impact of water vapor on NH_3 storage is performed using the same experimental setup described in Section 2.2. These studies begin by first adsorbing 400 ppmv of NH_3 in 3% H_2O. The inlet H_2O level is then raised to 11%, which results in a desorption of NH_3 from the binding of H_2O to the surface. After that step reaches equilibrium, the level of H_2O is subsequently reduced in a stepwise fashion to a final level of around 3%. Each decrease in H_2O concentration results in adsorption of NH_3. Integrating the difference between the inlet and outlet NH_3 during these experiments is used to determine how much additional NH_3 can be adsorbed at 400 ppmv when the water concentration is reduced. These experiments are done at the same isothermal temperatures as the capacity studies, but do not involve any TPDs at the end of the experiment.

2.5. Impact of aging

The experiments described in Sections 2.3 and 2.4 were repeated for the same Cu-SSZ-13 core sample under all aging conditions. Prior to any experiments, the Cu-SSZ-13 "de-greened" at 700 °C for 4 h in 10% O_2 and 10% H_2O. Then, after the experiments were run with the "de-greened" sample, the same sample was hydrothermally aged for a specified amount of time at 800 °C in 10% O_2 and 10% H_2O, and the NH3 storage experiments were repeated. This process was repeated to achieve cumulative aging time spans of 2, 4, 8, and 16 h.

3. Modeling Methods

3.1. Theoretical Considerations

Prior studies have used TPDs to show a distinction between NH_3 stored on Brønsted sites (ZH) and Cu sites. Based on this alone, there would need to be at least 2 distinct adsorption sites in the model.[5–9,14,18,25–29,32,37,38] However, other studies, including some density functional theory (DFT) analyses, indicate that the Cu sites are further divided into 2 distinct sites that can bind NH_3: (i) Z_1CuOH and (ii) Z_2Cu. [13,15,18,26,27,32,36,39,40] The Z_1 site represents a Cu ion associated with a single framework Al, while the Z_2 site represents a Cu ion associated with 2 framework Al. As a result, the Z_2 sites are generally considered more stable than Z_1 sites, and would therefore have different NH_3 adsorption energies.[39–41] Thus, the NH_3 storage model must involve at least 3 adsorption sites: (i) Z_1CuOH, (ii) Z_2Cu, and (iii) ZH.

To account for impacts of water vapor on NH_3 storage, the model needs a mechanism by which water vapor can adsorb and compete for storage sites in the Cu-SSZ-13 material. Computational work by Paolucci et al. [39,40] suggest that water vapor may adsorb to either Z_1CuOH or Z_2Cu. According to the DFT calculations, the Gibb's energy of reaction (ΔG_r) for the binding of a single water molecule on Z_1CuOH and Z_2Cu has a maximum difference in binding energy of less than 10 kJ/mol, indicating that, in the absence of NH_3, water would bind almost equally well on each Cu site [40], so the model needs to account for H_2O competition at both sites.

Additionally, while both Z_1CuOH and Z_2Cu bind NH_3, Z_2Cu sites are expected to bind more ammonia than Z_1CuOH sites.[31,37,40,42] According to theoretical and spectroscopic studies [40,42], the Z_2Cu site can solvate up to 4 NH_3 molecules at temperatures below 200 °C. Above this temperature, the coordination of NH_3 should be either 1 or 2 NH_3 molecules.[40] For Z_1CuOH, it is generally expected to coordinate only 1 NH_3 molecule within the temperature range examined in this work. [40] Thus, for simplification of the analysis, the model will consider Z_2Cu sites to bind twice as much NH_3 as the Z_1CuOH sites.

During hydrothermal aging, there can be a number mechanisms that impact NH_3 storage and overall SCR performance of the Cu-SSZ-13 material: (i) loss of ZH sites by interactions with mobile, inactive, or other Cu ions,[5,9,18,25,26] (ii) formation and/or re-dispersion of CuO, [6,18,41] and/or (iii) dealumination of the framework leading to structural collapse of the zeolite.[6] Aside from the possibility of structural collapse, the majority of proposed aging mechanisms seem to result in a shift or loss in site availability rather than fundamentally changing the binding affinities for NH_3 at those sites. Based on that, the aging component of the model could be developed to simply reflect a change in the site densities of Z_1CuOH, Z_2Cu, and ZH as a function of aging conditions and/or aging time.

3.2. Storage Model

Given the considerations outlined in Section 3.1, the model for NH_3 storage is developed from a set of 6 site-specific reactions:

$$NH_3 + Z_1CuOH \leftrightarrow Z_1CuOH\text{-}NH_3 \quad (1)$$

$$NH_3 + Z_2Cu \leftrightarrow Z_2Cu\text{-}NH_3 \quad (2a)$$

$$NH_3 + Z_2Cu\text{-}NH_3 \leftrightarrow Z_2Cu\text{-}(NH_3)_2 \quad (2b)$$

$$NH_3 + ZH \leftrightarrow ZNH_4 \quad (3)$$

$$H_2O + Z_1CuOH \leftrightarrow Z_1CuOH\text{-}H_2O \quad (4a)$$

$$H_2O + Z_2Cu \leftrightarrow Z_2Cu\text{-}H_2O \quad (4b)$$

Reactions 1 and 2 account for NH_3 storage that is split between the 2 unique Cu binding sites. Reaction 2 is sub-divided into 2a and 2b to represent the binding of additional NH_3 at that site. Reaction 3 accounts

for binding of NH_3 to Brønsted sites. The binding of water to Cu sites is represented by reaction 4, which is sub-divided into 4a for binding to Z_1CuOH and 4b for binding to Z_2Cu. Binding of water to Brønsted sites is not considered in this model because the Brønsted sites are expected to vastly out-compete water for these sites given the very high release temperatures of NH_3 from Brønsted sites that are indicative of strong binding interactions.[5–9,14,18,19,21,25–29].

Total molar capacity (q_T) of the material for NH_3 (Eq. 5) is then calculated from the sum of the NH_3 bound to each site (q_i) and will be a function of the binding affinities for each site (K_i), the initial site densities (w_i), and the gas-phase concentrations of NH_3 and H_2O (C_i). Eq. 6, 7, and 8 provide the functions for the capacities of each site, where site 1 is Z_1CuOH, site 2 is Z_2Cu, and site 3 is ZH. For Eqs. 6 and 8, the functions are straightforward applications of the Extended Langmuir and single-site Langmuir functions, respectively.[43] Eqs. 7a through 7b was derived from reactions 2a, 2b, and 4b by taking into account the molar amounts of NH_3 bound to that site by each reaction and the total site balance based on all possible surface species for that site. A derivation of Eqs. 7a through 7d is provided in Supplemental Information.

$$q_T = q_1 + q_2 + q_3 \tag{5}$$

$$q_1 = w_1\left(\frac{K_1 C_{NH_3}}{1 + K_1 C_{NH_3} + K_{4a} C_{H_2O}}\right) \tag{6}$$

$$q_2 = w_2 \bullet \alpha \bullet (1-\beta) + 2 \bullet w_2 \bullet \beta \tag{7a}$$

$$\alpha = \left(\frac{K_{2a} C_{NH_3} \bullet (1-\gamma)}{1 + K_{2a} C_{NH_3} \bullet (1-\gamma)}\right) \tag{7b}$$

$$\beta = \left(\frac{K_{2a} K_{2b} C_{NH_3}{}^2 \bullet [(1-\alpha)\bullet(1-\gamma)]}{1 + K_{2a} K_{2b} C_{NH_3}{}^2 \bullet [(1-\alpha)\bullet(1-\gamma)]}\right) \tag{7c}$$

$$\gamma = \left(\frac{K_{4b} C_{H_2O}}{1 + K_{4b} C_{H_2O}}\right) \tag{7d}$$

$$q_3 = w_3\left(\frac{K_3 C_{NH_3}}{1 + K_3 C_{NH_3}}\right) \tag{8}$$

The NH_3 storage model developed here is mathematically similar to models developed by Olsson et al. [33,34] and Gao et al. [35] for NH_3 storage on Cu-SSZ-13, but has some notable differences. Each model uses distinct adsorption sites for NH_3 binding in a Langmuir-like series of reactions. However, the physical interpretation of each of those sites is different between those papers and the model presented here. In Eqs. 1 through 3 of this work, each site is specific to either a particular Cu ion or is a Brønsted site. Both Olsson et al. [33,34] and Gao et al. [35] combine the storage of NH_3 at Brønsted sites with storage at Cu sites in the same site term. In other words, neither Olsson et al. [33,34] nor Gao et al. [35] provide a clear separation between the amount of ammonia stored at Brønsted sites and the amount stored at copper sites. Thus, while each model uses a similar mathematical schema for representing binding, the physical interpretation of the binding at each models' own sites is different. This may be problematic for modeling specific aspects of NH_3 storage, such as TPDs, as it is understood that the energetics for the binding at each site can be different.[39,40].

3.3. Transient Model

In addition to the formulation of the storage model, a transient kinetic model for NH_3 storage can be developed from the reactions outlined in Eq. 1 through 4. The rates for each reaction would then follow the general formula outlined in Eq. 9. In this expression, the rate of formation (r_i) of the adsorbed species (q_i) is a function of forward ($k_{f,i}$) and reverse ($k_{r,i}$) rate constants, the concentration of the adsorbate (C_j), and the availability of the specific reaction site (S_k). Note that given this formulation, the partially solvated Z_2Cu-NH_3 species would also be an available site for the additional of another NH_3 molecule. If it is assumed that the reaction rate constants obey the Arrhenius rate expression (Eq. 10), and the adsorption enthalpies (ΔH_i) and entropies (ΔS_i) are known for each reaction, then only the forward Arrhenius rates terms ($A_{f,i}$ and $E_{f,i}$) need to be determined to solve for the reverse terms (Eqs. 11 and 12).[33,34].

$$r_i = k_{f,i} C_j S_k - k_{r,i} q_i \tag{9}$$

$$k_{f,i} = A_{f,i} \bullet \exp\left\{-\frac{E_{f,i}}{RT}\right\} \tag{10}$$

$$E_{r,i} = E_{f,i} - \Delta H_i \tag{11}$$

$$A_{r,i} = A_{f,i} \bullet \exp\left\{-\frac{\Delta S_i}{R}\right\} \tag{12}$$

Once the reaction kinetics are formulated, those terms can be put into an overall transient model to account for mass transport/transfer and reactions occurring inside the catalyst reactor system described in Section 2. To model this system, there are 2 classical approaches: (i) a 1D–1D axial transport and pore diffusion model or (ii) a 1D–0D axial transport and effective mass-transfer/pore-diffusion model.[33,34,44–47] For simplicity, the 1D–0D type model is adopted here in this study, which is a model that neglects intralayer diffusion limitations. A justification of this simplification is made by checking the Weisz-Prater criterion [48] and calculations of this criterion are provided in Supplemental Information. This model is represented mathematically as shown in Eqs. 13 through 14. Note that the energy balance is ignored here since the catalyst was kept isothermal through the experiments.

$$\varepsilon_b \frac{\partial C_{b,i}}{\partial t} + \nabla \bullet \left(\varepsilon_b v C_{b,i}\right) = -G_a k_{m,i}\left(C_{b,i} - C_i\right) \tag{13}$$

$$\varepsilon_w (1-\varepsilon_b)\frac{dC_i}{dt} = G_a k_{m,i}\left(C_{b,i} - C_i\right) - (1-\varepsilon_b)\sum_{\forall j} u_j r_j \tag{14}$$

Eq. 13 represents the transport of adsorbate species in the bulk gas phase ($C_{b,i}$) of the monolith system. That transport is a function of the bulk void space (ε_b), the average gas velocity (v), the surface area to volume ratio for the catalyst (G_a), and the effective mass-transfer rate ($k_{m,i}$).[33,34,44] That transport is coupled to the average concentration in the pore-space (C_i) of the washcoat of the catalyst monolith (Eq. 14) and is a function of the washcoat porosity (ε_w), the mass-transfer from the bulk space, the molar stoichiometry of additional adsorbed NH_3 for that reaction (u_j), and the rate reactions (r_j) that result in uptake of NH_3 at the set of specific adsorption sites.[45].

The transient model described in Eqs. 13 and 14 was developed as an application built on the Multiphysics Object-Oriented Simulation Environment (MOOSE), a finite element modeling framework developed at Idaho National Laboratory.[49] For stability and localized mass conservation, the advective terms of the transport problem were discretized using Discontinuous Galerkin finite elements with first order monomial shape functions.[50] Integration in time was performed iteratively using a standard implicit Euler scheme with a Jacobian-Free Newton-Krylov method [51] preconditioned with a full single matrix preconditioner. Source code for the MOOSE application, named Catalytic After Treatment System (CATS), developed in this work can be obtained from a public GitHub repository.[52].

3.4. Aging Model

The aging model will address the changes in each site capacity by adjusting the individual site densities (w_i) as a function of aging conditions and time. From multiple literature sources, it is understood that there is a transformation of active ZH sites to active Cu sites for NH_3 binding during the aging process.[5,9,18,25,26] This type of transformation is the basis behind the "de-greening" practice to prepare

materials prior to use by increasing the levels of active Cu sites.[18] Also, this would imply that there are Cu species within the material that may be inactive for NH_3 storage and/or NOx reduction until the materials have undergone some degree of hydrothermal aging. Additional studies have shown that a Z_1 Cu species can become a Z_2Cu site when a Brønsted site reacts with a Z_1 Cu species.[25,40,41,53] This would then result in a shift from NH_3 capacity on ZH and Z_1CuOH to NH_3 capacity at Z_2Cu. Under extended hydrothermal aging times, an equilibrium distribution between Z_1 and Z_2 sites can be achieved. The ultimate distribution between these types of sites is a function of both the Si-to-Al and Cu-to-Al ratio of the material.[39,40] This type of aging mechanism can be represented by Eq. 15.

$$ZH + Z_1CuOH \leftrightarrow Z_2Cu + H_2O \tag{15}$$

In addition to the mechanism for a loss of ZH and gain of Z_2Cu, prior studies have shown that the Z_1CuOH sites, which are less stable than Z_2Cu sites, can be lost to the formation of CuO clusters during hydrothermal aging.[6,18,26,41] However, other studies have noted that there is no appreciable amount of CuO formed during aging [27] or that CuO species may even migrate to acid sites to form active Cu sites.[54] Given these considerations, the model developed here will consider this aging mechanism as a reversible reaction between a ZH and CuO species to form a Z_1CuOH site (Eq. 16).

$$ZH + CuO \leftrightarrow Z_1CuOH \tag{16}$$

One thing to note about the above aging reactions is that while they represent a shifting of the NH_3 storage sites with aging, they do not necessarily result in a loss in capacity. Thus, these two mechanisms on their own would be insufficient to describe the ammonia capacity losses seen in the literature and in our ammonia storage data. Thus, a third aging mechanism must be introduced. There is experimental evidence from TPDs suggesting that there is some net loss in total NH_3 storage capacity with aging.[18–21,25,26] The majority of the net losses seem to come from a reduction in Brønsted sites as the high temperature peaks of the TPDs degrade faster than the low temperature peaks increase. Based on this, there is likely some additional aging mechanism wherein solitary Brønsted acid sites are lost during hydrothermal aging. The simplest way to represent these losses would be through an irreversible reaction of ZH sites (Eq. 17). Note that this equation is purely empirical in nature and is not meant to represent dealumination, since the Al is not being removed from the framework. The physical interpretation of this is just a general loss of Brønsted acidity in the zeolite and this reaction is not meant to represent any specific chemical mechanism or pathway for this loss.

$$ZH + 0.25\ O_2 \rightarrow Z + 0.5\ H_2O \tag{17}$$

Using the set of three aging reactions, a system of differential equations can be derived to represent the rates of change for each binding site during hydrothermal aging (Eqs. 18 through 20). Each rate is assumed first order with respect to the concentrations of sites and orders with respect to the gases (H_2O and O_2) are set to zero. This is because the concentrations of H_2O and O_2 were left constant during the aging protocols. Those rate parameters would then represent a specific set of rate values under the hydrothermal aging conditions outlined in this work and obtained by fitting the changes in site densities at those conditions.

$$\frac{d[ZH]}{dt} = -k_1[ZH][Z_1CuOH] + k_{-1}[Z_2Cu] - k_2[ZH][CuO] + k_{-2}[Z_1CuOH] - k_3[ZH] \tag{18}$$

$$\frac{d[Z_1CuOH]}{dt} = -k_1[ZH][Z_1CuOH] + k_{-1}[Z_2Cu] + k_2[ZH][CuO] - k_{-2}[Z_1CuOH] \tag{19}$$

$$\frac{d[Z_2Cu]}{dt} = k_1[ZH][Z_1CuOH] - k_{-1}[Z_2Cu] \tag{20}$$

Daya et al. [32], Olsson et al. [33], and Supriyanto et al. [55] have also adapted their NH_3 storage and SCR reaction models to account for aging. Similar to the approach of this work, Daya et al. [32] and Supriyanto et al. [55] adjust the site densities of the NH_3 storage sites depending on the aging conditions. However, Supriyanto et al. [55] also adjusted the site energetics as a function of aging. Theoretically, the binding strengths should not change with aging time [5,9,18,25,26], so the need for adjustments in the site enthalpies from the model by Supriyanto et al. [55] may be a consequence of not fully separating out the Brønsted sites from the Cu sites in their reaction equations.

4. Results

4.1. Ammonia Storage

Data collected for NH_3 storage capacities under all conditions were analyzed using non-linear least squares regressions to ascertain the enthalpies (ΔH_i) and entropies (ΔS_i) for each storage reaction (Eq. 1 through 4). Those reaction energies were adjusted during the regression analysis and used to calculate the binding constants for each reaction (K_i) using the van't Hoff relationship (Eq. 21). The regression analysis was constrained to ensure that the enthalpies and entropies would not change with aging conditions. Instead, only the site densities (w_i) were allowed to vary across the various aging conditions to account for the impact of hydrothermal aging on site availability. All regression analyses were performed using the Solver functionality of Excel with the Generalized Reduced Gradient (GRG) method.

$$ln(K_i) = -\frac{\Delta H_i}{RT} + \frac{\Delta S_i}{R} \tag{21}$$

The resulting optimal reaction energies are provided in Table 2 and the optimal site densities for each aging condition are given in Table 3. Modeling the NH_3 inventory using these tabulated values provides the comparisons shown in Figs. 1 through 3 (and Figures A1 and A2 in Supplemental Information). Each figure shows (a) the isotherms of NH_3 storage versus NH_3 partial pressures at 5% H_2O concentration and (b) the capacities for NH_3 storage at 400 ppmv NH_3 versus various H_2O partial pressures. Overall, the model does well to capture all storage data under all experimental conditions.

4.2. Impact of Aging

The results from Figs. 1 through 3 (and Figures A1 and A2 in Supplemental Information) demonstrate that it is feasible to capture the impact of hydrothermal aging on NH_3 storage simply by adjusting the number of available storage sites without the need to change any site energies, confirming the hypothesis used in building the storage model. To capture this change in site densities, the aging model proposed in Eqs. 15 through 17 was used in conjunction with the site densities reported in Table 3 to find optimal aging parameters and rates for each reaction. Data analysis was performed by numerically integrating Eqs. 18 through 20 from 0 to 16 h of hydrothermal aging, then adjusting each rate coefficient (k_1, k_{-1}, k_2, k_{-2}, and k_3) to obtain the best fit of the site densities by minimization of the Euclidean norm. The initial site densities for Z_1CuOH, Z_2Cu, and ZH were assumed to be w_1, w_2, and w_3, respectively, for the unaged condition. The initial amount of CuO was approximated

Table 2
Summary of optimal site energies for each reaction in Eq. 1 through 4.

Reaction	1	2a	2b	3	4a	4b
ΔH_i (kJ/mol)	-54.5	-78.1	-78.1	-91.9	-32.1	-28.9
ΔS_i (J/K/mol)	-30.0	-35.3	-46.8	-28.9	-24.2	-26.7

Table 3
Summary of optimal site densities for each aging condition/time.

Aging Time	w_1 (mol/L)	w_2 (mol/L)	w_3 (mol/L)
"Unaged"	0.0526	0.0231	0.0263
2 hrs	0.0513	0.0258	0.0183
4hrs	0.0497	0.0269	0.0142
8 hrs	0.0484	0.0267	0.0117
16hrs	0.0503	0.0252	0.0093

by the fitting routine. Results from the aging data analysis are provided in Table 4 and Fig. 4.

4.3. Temperature Programmed Desorption

At the end of each isothermal NH_3 concentration variation experiment, a TPD was performed to desorb all remaining NH_3 on the catalyst by stopping the NH_3 flow and ramping the temperature linearly from the experiment temperature to around 550 °C. A selection of the TPD curves are shown in Fig. 5 for the de-greened catalyst. Fig. 5 shows that the TPDs collected in this study show a clear 2-peak profile as expected. It also shows that the low temperature peak undergoes significant decline as the temperature of the storage experiment was increased. As noted previously, the low temperature peak corresponds to the NH_3 storage on Cu sites, whereas the high temperature peak corresponds to NH_3 storage on Brønsted acid sites.[5–9,14,18,25–29,32] These TPD results in Fig. 5 have a higher desorption peak at lower temperature, which indicates that there is more NH_3 on Cu sites. This finding is consistent with the storage model that found there are significantly more total Cu sites available than Brønsted acid sites (Table 3).

In addition, the aging model and data analysis developed in this work indicates that there is a significant loss in Brønsted acid sites with a corresponding increase in Cu sites (Fig. 4). This phenomenon is mirrored in the TPD data as well. Fig. 6 shows the TPD profiles across all aging conditions for the 150 °C isotherm data set. The 150 °C data set is used in this analysis since that temperature had the most pronouced 2-peak featured TPD from Fig. 5. Fig. 6 clearly shows that the high temperature peak is significantly less pronouced after hydrothermal aging, which indicates a loss in Brønsted acid sites with aging. At the same time, the low temperature peak, which corresponds to NH_3 storage on Cu sites, increases in intensity. This indicates that there is a gain in Cu sites with hydrothermal aging. Both of these phenomena are captured in the aging model (Fig. 4) that shows the majority of the site transformations occur in the first 2 h of aging. Additionally, there is a

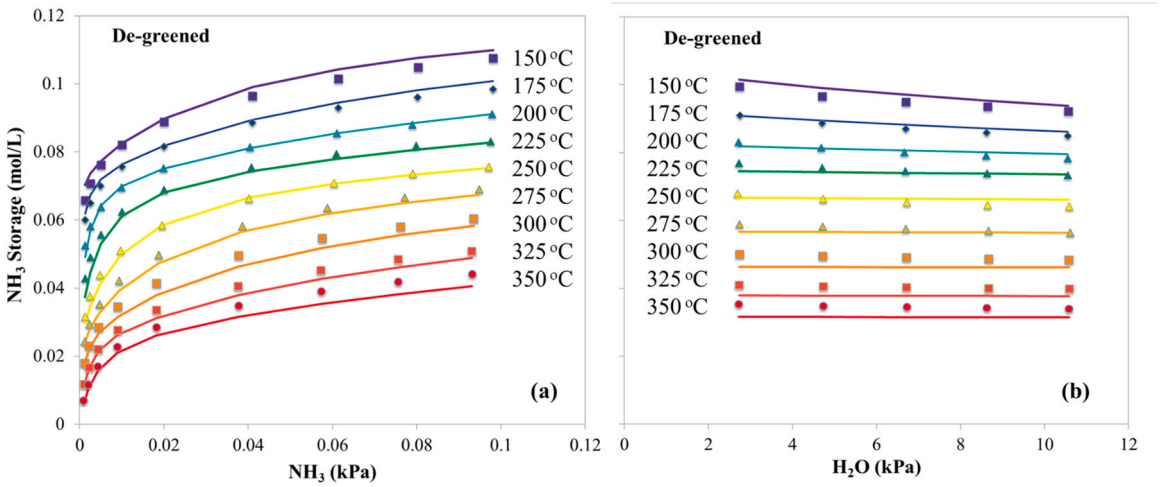

Fig. 1. Measured (points) and simulated (lines) NH_3 inventory as a function of (a) NH_3 partial pressures with 5% H_2O and (b) H_2O partial pressures with 400 ppmv NH_3 for a de-greened Cu-SSZ-13 sample.

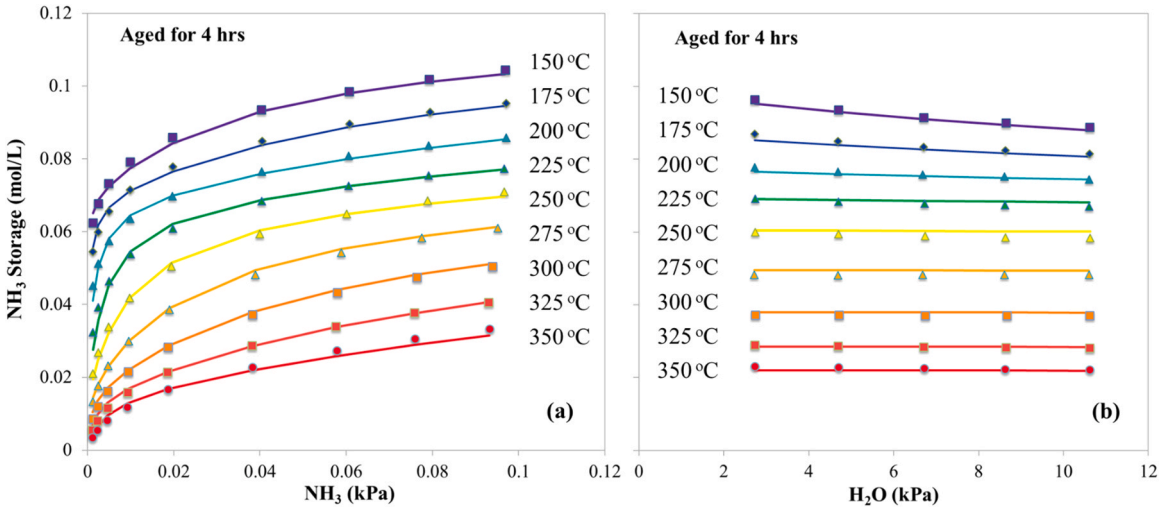

Fig. 2. : Measured (points) and simulated (lines) NH_3 inventory as a function of (a) NH_3 partial pressures with 5% H_2O and (b) H_2O partial pressures with 400 ppmv NH_3 for a Cu-SSZ-13 sample aged at 800 °C for 4 h.

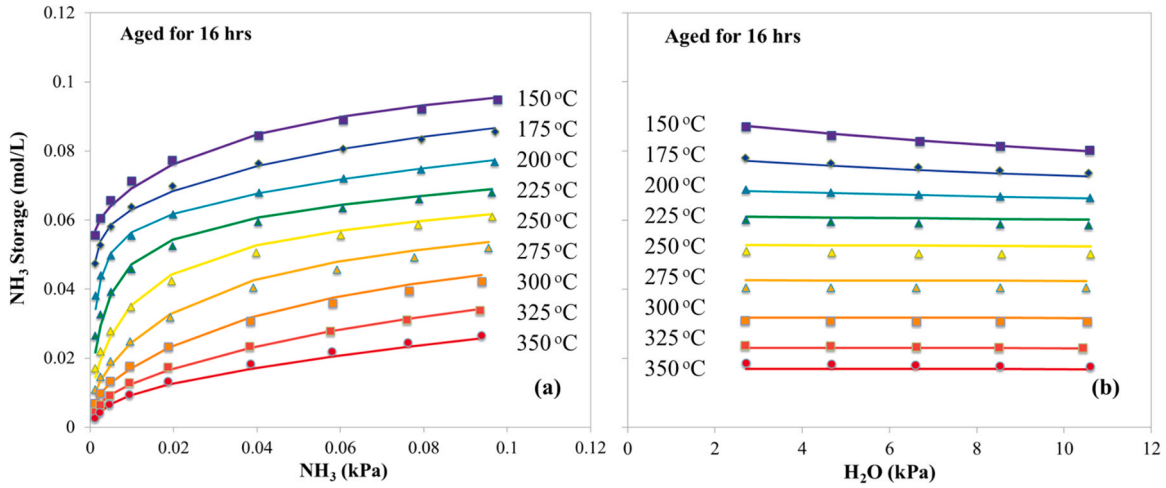

Fig. 3. : Measured (points) and simulated (lines) NH_3 inventory as a function of (a) NH_3 partial pressures with 5% H_2O and (b) H_2O partial pressures with 400 ppmv NH_3 for a Cu-SSZ-13 sample aged at 800 °C for 16 h.

Table 4
Summary of optimal aging reaction rates and initial site densities of the aging model.

Rate Parameters (*hr^{-1})	
k_1	2.4609
k_{-1}	0.0532
k_2	170.78
k_{-2}	0.0008
k_3	0.0676
Initial Site Densities (mol/L)	
$[Z_1CuOH]_o$	0.0526
$[Z_2Cu]_o$	0.0231
$[ZH]_o$	0.0263
$[CuO]_o$	0.0011

*Units are per hour of aging time.

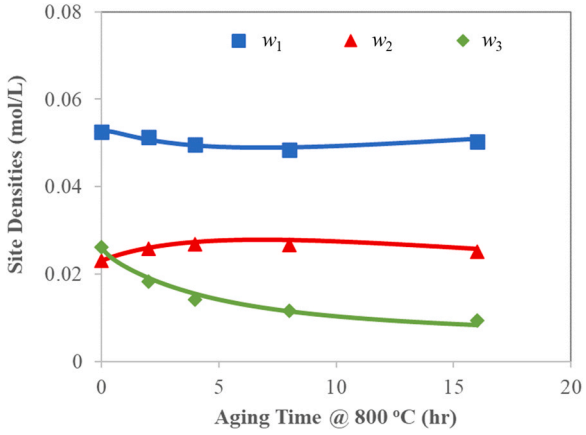

Fig. 4. Variations in site densities (points) with aging time along with the simulated aging densities (lines) from the aging model and optimal aging parameters in Table 4.

noticeable drop in the low temperature peak from 8 h to 16 h. This may be a result of CuO formation with extended hydrothermal aging, however, it is difficult to assess whether or not this observed drop is a trend or an outlier. More experimental work beyond 16 h of hydrothermal aging may be necessary to assess this.

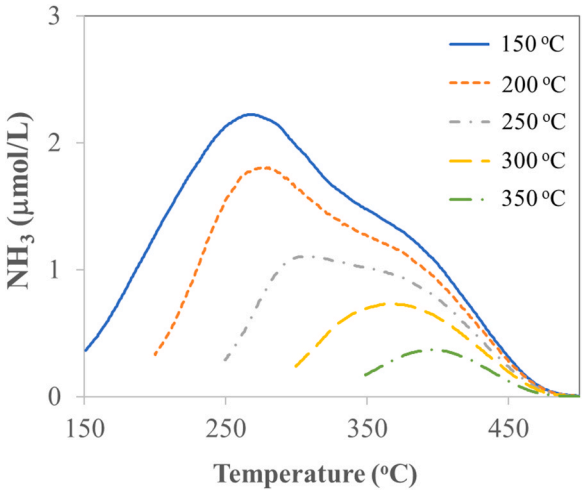

Fig. 5. Measured TPD profiles for the de-greened Cu-SSZ-13 material.

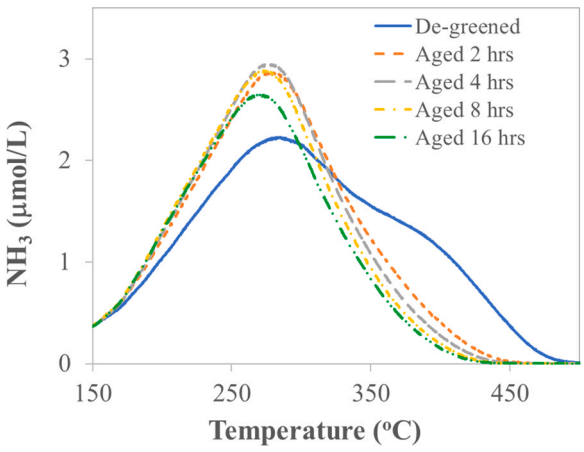

Fig. 6. Measured TPD profiles after 150 °C storage experiments for all aging conditions.

4.4. Transient Model Simulations

To simulate the transport, adsorption, and desorption of NH_3 in the catalyst system there are a number of parameters that need to be determined or approximated before the kinetic rate parameters for each reaction can be found by fitting a subset of the data. The cross-sectional area of the monolith samples is roughly 33% voids ($\varepsilon_b = 0.33$) and the average gas velocity (v) was estimated from the total volumetric flow rate (Q) divided by the cross-sectional void area ($\varepsilon_b \pi r^2$, where r is the radius of the monolith). In this work, the volumetric flow rate was fixed to achieve a GHSV of 30,000 h^{-1}.

The surface area to volume ratio for a monolith can be calculated from the cell-density of the monolith and the hydraulic diameter of the channels.[33,44,45] Given that the cell-density of the monolith in this work was about 400 cells/in^2, the hydraulic diameter can then be approximated to roughly 0.077 cm. This results in an approximate ratio of 1928 m^{-1} (in surface area per total volume) for G_a in the Cu-SSZ-13 monolith used in this study. Calculations for hydraulic diameter and G_a are provided in Supplemental Information. For the washcoat porosity (ε_w), a typical value of 0.4 was assumed. The effective mass transfer coefficient ($k_{m,i}$) can be calculated from the Sherwood number Sh $= d_h k_{m,i}/D_{eff}$), which correlates pore-diffusivity with hydraulic diameter. For a Cu-SSZ-13 monolith and a gas flow rate corresponding to a GHSV of 30,000 h^{-1}, values for pore-diffusivity and Sherwood number have been calculated to be 2×10^{-5} m^2/s and 2.7 at 150 °C, respectively, resulting in a mass transfer coefficient of about 4.04 m/min. This value will increase with temperature as the Sherwood numbers and diffusivities change. Methods and equations for calculating Sherwood numbers and mass transfer coefficients are provided in Supplemental Information.

To determine the reaction rate coefficients requires some fitting of the transient data with the model outputs from Eqs. 13 and 14. However, this analysis can be simplified by assuming the activation energies for the forward half of the adsorption reactions ($E_{f,i}$) are all zero, which is in line with prior work on NH_3 adsorption.[33,34] Additionally, this convention places a strict constraint on the optimization of the kinetics and reduces the possibility that the data becomes overfit. This means that only the pre-exponential rate parameters for the forward reactions ($A_{f,i}$) need to be determined. In addition, since all the reactions proposed are the same regardless of aging condition, only the de-greened transient data will be used to adjust those rate parameters. All subsequent simulations for the aged cases will then be predictions based on the optimal rates from the de-greened data set.

Table 5 summarizes the activation energies and pre-exponential terms from the transient data analysis for de-greened Cu-SSZ-13. The pre-exponential factor order-of-magnitudes found in this study are relatively close to those found in Olsson et al. [33,34] for the high and low temperature NH_3 adsorption reactions. Fig. 7 shows the comparison between the simulated and actual transient data for de-greened Cu-SSZ-13 at various temperatures. Additional and enlarged figures are provided as Supplemental Information (Section 2).

Using the reaction rate parameters (Table 5) determined from the unaged data analysis and the variations in each site density from the aging analysis (Fig. 4), the model was then used to predict the transient data results for all the aged Cu-SSZ-13 experimental runs. Selected results from these simulations are provided in Figures 11 through 14. Additional and enlarged figures are provided as Supplemental Information (Sections 2 through 7), as well as some kinetic plots for the desorption/adsorption cycles caused by changing the H_2O inlet levels. These results indicate that the data analysis with only the unaged data to find rate parameters was likely sufficient for predicting the TPDs and adsorption-desorption behavior of the catalyst monoliths.

Table 5
Summary of reaction rate parameters from data analysis of unaged transient data.

Reaction	$E_{f,i}$ (kJ/mol)	$A_{f,i}$ (L/mol/s)
Eq. (1)	0	4.2×10^3
Eq. (2a)	0	5.0×10^3
Eq. (2b)	0	2.5×10^3
Eq. (3)	0	4.2×10^4
Eq. (4a)	0	7.3×10^2
Eq. (4b)	0	1.2×10^3

5. Discussion

The NH_3 storage model developed in this work did extraordinarily well at describing all NH_3 inventories under all conditions and was able to do so without needing to vary the site energies with aging conditions. This is consistent with prior theoretical and experimental work that has described the aging as only impacting site availability and not binding strength.[5,9,18,25,26] In addition, the model was capable of adequately describing reductions in NH_3 storage caused by the addition of higher concentrations of water vapor. Both the model and data showed that there is only a minor impediment that water vapor has on NH_3 storage at the lowest temperatures and virtually no impact on NH_3 storage at higher temperatures (Figs. 1 through 3, and Figures A1 and A2 in Supplemental Information).

The optimal site energies (ΔH_i and Δ_{Si}) determined from the data analysis are also consistent with discussions in the literature.[39,40] Comparing the binding energies for NH_3 on Z_1CuOH and Z_2Cu (Table 2) it can be seen that NH_3 is more stably bound to Z_2Cu than Z_1CuOH, as indicated by the variations in the estimated enthalpies. In addition, water vapor forms a weaker bond with Cu sites than NH_3. This observation is consistent with calculations by Paolucci et al. [39,40] and helps to explain why the impact of water vapor on NH_3 storage is minor. It is also worth noting that the strongest binding occurs between NH_3 and Brønsted sites, which is consistent with TPD observations in this study and others that show desorption from Brønsted sites occurs at higher temperatures compared to Cu sites.[5–9,14,18,25–29,32].

Results from the site density analysis shows that the unaged Cu-SSZ-13 material contains 0.076 mol/L of active Cu sites (Z_1CuOH and Z_2Cu) for NH_3 binding and 0.0263 mol/L of total Brønsted acid sites. If it is assumed that all Cu associated with 1 framework Al is represented solely by the amount of Z_1CuOH sites, then the molar ratio of single framework Al-Cu species to the total-Cu species would be approximately 0.69. This ratio should theoretically be a function of the Si/Al ratio and Cu/Al ratio of the material. According to Paolucci et al. [40], a Cu-SSZ-13 catalyst with the same Si/Al and Cu/Al ratios as this material (SiAl = 15 and CuAl = 0.42) would result in a Z_1Cu-to-total Cu somewhere around 0.75. This indicates that the single Al-Cu species to total-Cu species estimated in this work is relatively consistent with theory and only deviates by about 8% from the expected value.

The aging model (Eqs. 15 through 17) captures the changes in site density well (Fig. 4). Initially, the Cu-SSZ-13 material has a significant amount of Brønsted acid sites, but loses most of those sites to the formation of Z_2Cu sites. This result is also mirrored in the TPDs at the various aging conditions (Fig. 6). After the first 2 h of hydrothermal aging, the high temperature TPD peak is nearly completely lost, while the low temperature peak increases in intensity. Further hydrothermal aging continues to have an impact, however, that impact is much less significant beyond the initial 2 h (Fig. 6). This is in line with the aging model (Fig. 4) which also shows the bulk of hydrothermal aging impacts are felt within the first 2 h of aging.

Comparisons between the transient model and data (Figs. 7 through 9, and Figures A3 and A4 in Supplemental Information) show good agreement as well. The breakthrough times at initial loading and the stepwise desorption regions show excellent agreement across all data sets. Most of the simulated TPDs show reasonable agreement with the data, however, there are some notable discrepancies in the TPDs for the de-greened sample at the lowest isothermal temperatures. Qualitatively, the simulated TPDs in this region show what is expected, a high

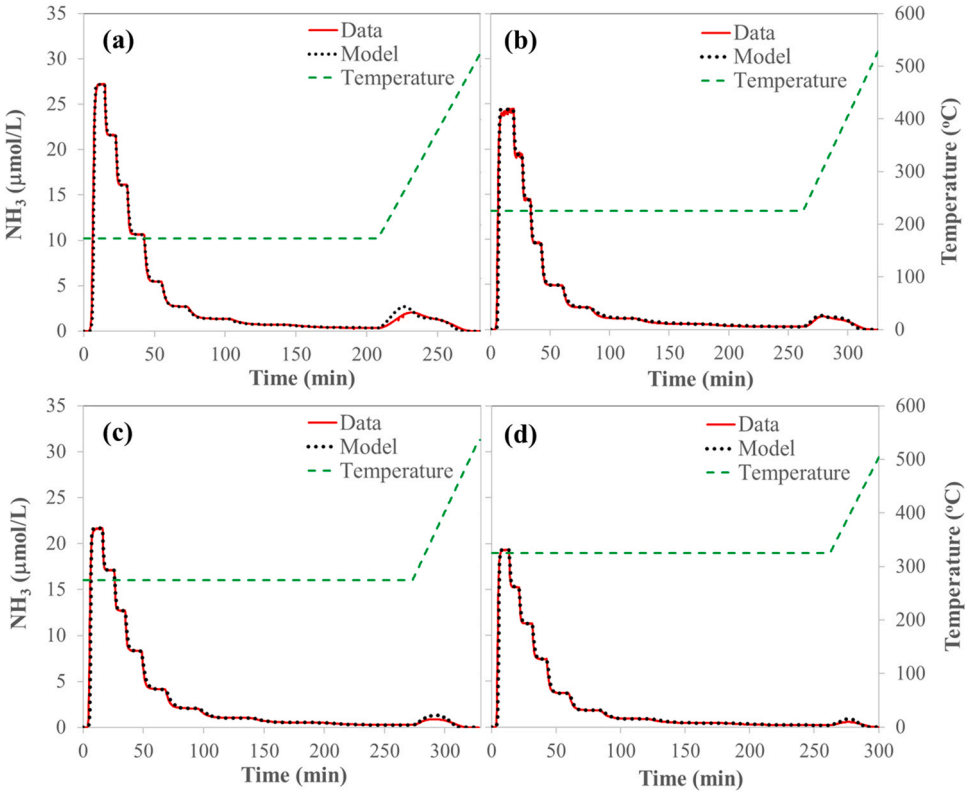

Fig. 7. Select transient NH_3 concentration data (red solid line) and simulation results (black dashed line) for de-greened Cu-SSZ-13 during NH_3 storage and release experiments at (a) 175 °C, (b) 225 °C, (c) 275 °C, and (d) 325 °C.

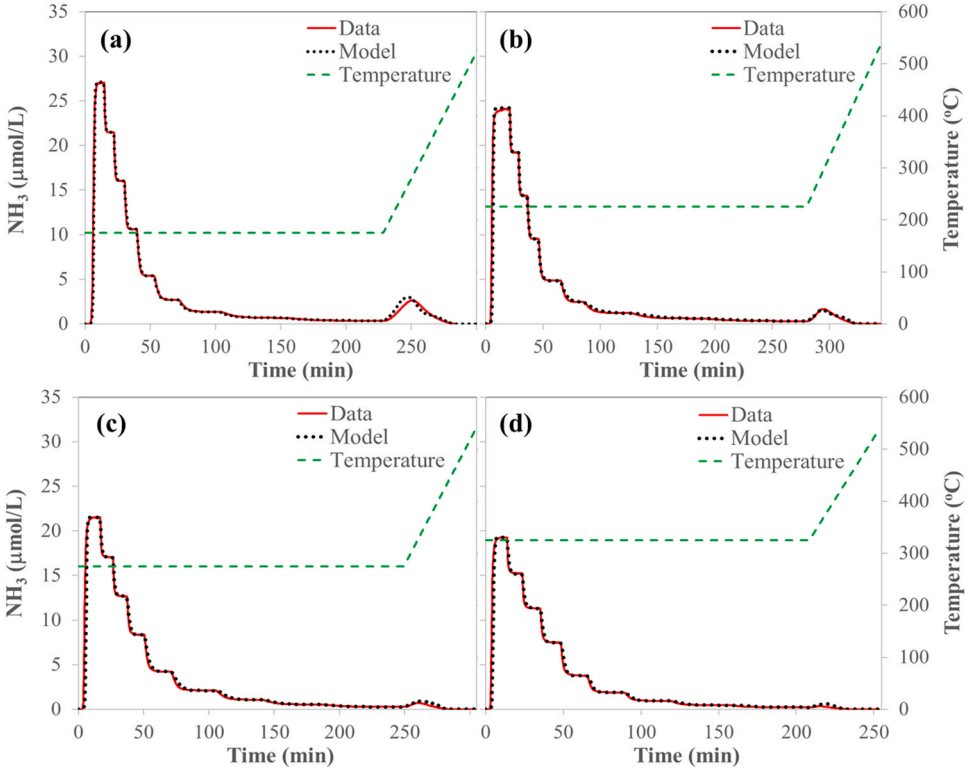

Fig. 8. : Select transient NH_3 concentration data (red solid line) and simulation predictions (black dashed line) for Cu-SSZ-13 aged 4 h at 800 °C during NH_3 storage and release experiments at (a) 175 °C, (b) 225 °C, (c) 275 °C, and (d) 325 °C.

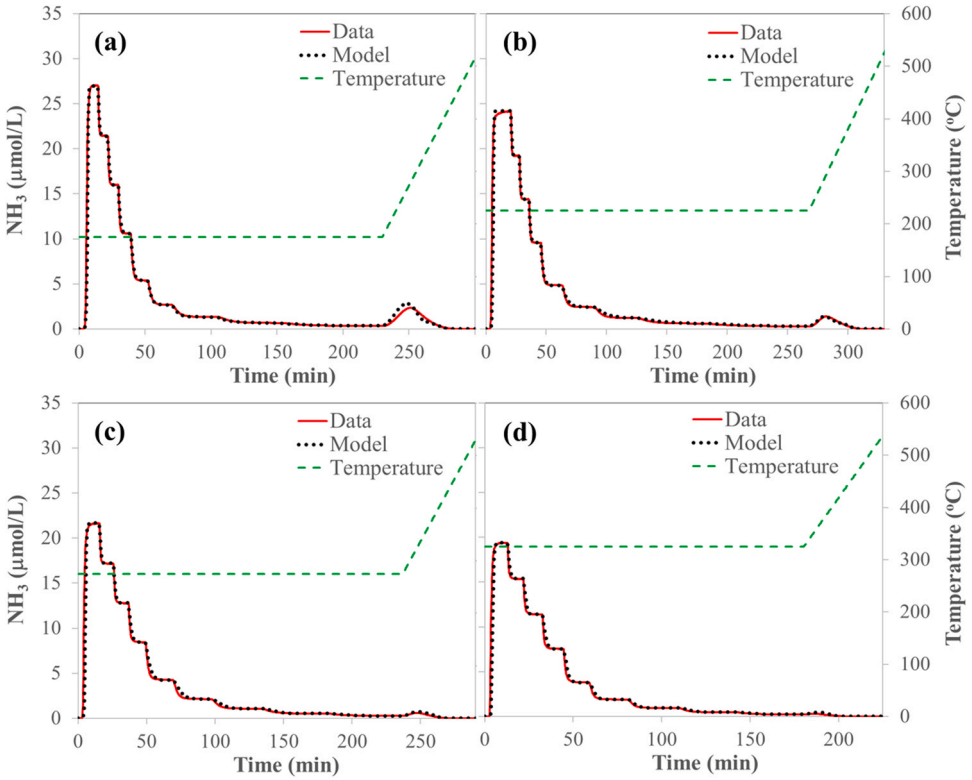

Fig. 9. : Select transient NH_3 concentration data (red solid line) and simulation predictions (black dashed line) for Cu-SSZ-13 aged 16 h at 800 °C during NH_3 storage and release experiments at (a) 175 °C, (b) 225 °C, (c) 275 °C, and (d) 325 °C.

desorption peak at low temperature and a smaller peak or shoulder feature at the higher temperature, but quantitatively the model simulates more desorption of NH_3 in the low temperature region than is actually observed. This is likely caused by errors associated with the isothermal storage predictions at low NH_3 concentration and low temperature. As can be seen in Fig. 1, the storage model overestimates the NH_3 storage at the lowest temperatures and partial pressures. This would then translate to an overestimation of desorption of NH_3 during the TPD stage of the transient model. Similar errors are seen in the aged capacities at the lowest temperature and partial pressures (Figs. 3 through 6), however, those are significantly smaller, which results in better agreement between measured and simulated TPDs for the aged sample data (Figs. 8 and 9, and Figures A3 and A4 in Supplemental Information).

6. Conclusion

In this work, adsorption and desorption studies were performed to assess the NH_3 storage on a commercial Cu-SSZ-13 catalyst under various conditions. Isothermal temperatures were varied between 150 and 350 °C while the NH_3 exposure concentrations varied from 12.5 to 1000 ppmv. During the capacity evaluations, the H_2O content was held constant at about 5%. Additional experiments were performed to assess the impact that variations in water vapor content would have on the NH_3 capacity of Cu-SSZ-13. For these studies, the NH_3 concentration was held to 400 ppmv and the H_2O concentrations were varied from 3% to 11% for all previous isothermal temperatures. All of the above experiments were performed with a de-greened Cu-SSZ-13 catalyst and then after the catalyst was hydrothermally aged at 800 °C (with 10% O_2 and 10% H_2O) for 2, 4, 8, and 16 h total.

Models for NH_3 storage, aging mechanisms, and transient behavior of NH_3 adsorption were developed in this work to simulate the changes in NH_3 storage on Cu-SSZ-13 under the various experimental conditions and aging times. These models were developed based on an in-depth literature review of the reaction pathways and mechanisms for NH_3 binding on Cu sites and Brønsted acid sites in the materials. The resulting capacity model was created as the function of 6 Langmuir-like reactions (Eq. 1 through 4) in which NH_3 can bind to 3 different sites in the chabazite with additional reactions representing the competition for the Cu sites by water vapor. Results from the data analysis with this model (Figs. 1 through 3, and Figures A1 and A2 in Supplemental Information) demonstrate that these 6 reactions are sufficient to describe both the isothermal capacities and the impact of water on NH_3 binding for a wide range of conditions. Furthermore, the hypothesis that aging effects on NH_3 storage can be captured by simply adjusting site densities was confirmed.

The aging model was constructed from three reactions (Eqs. 15 through 17) to account for the transformation of Brønsted sites to Z_2Cu sites, the formation of CuO species, and an empirical general loss of Brønsted acidity through aging. This model was able to adequately describe the changes in the site densities with hydrothermal aging (Fig. 4). Results indicated that the majority of the aging occurred within the first 2 h and that there was a small gain in Z_2Cu sites corresponding to a loss of Brønsted sites through the mechanism in Eq. 9. This observation was also mirrored in the TPDs for each aging condition (Fig. 6) that clearly show a loss in high temperature storage of NH_3 with a gain in low temperature storage.

Storage and aging models were integrated into a transient model (Eqs. 13 and 14) to simulate the full data sets produced in this work. Comparisons with the unaged data sets were used to estimate the reaction rates for the storage model (Table 5). Those estimated rates were then applied to predict the transient behavior for all aged data sets. The results showed very good agreement with the data and provide additional validation that the models developed in this work are adequate for predicting NH_3 capacity and kinetics in Cu-SSZ-13 under various conditions.

The data and models produced by this work are integral components to modeling and understanding the overall NOx conversion process for

SCR. This is because NH_3 storage has a significant impact on NOx conversion as the NOx needs to react with NH_3 bound to Cu sites in the catalyst to be reduced to N_2. Thus, accurately predicting the amount of NH_3 stored in the catalyst, and at which sites ammonia is stored, is needed to also predict the NOx conversion efficiency of the materials under various operating conditions.

CRediT authorship contribution statement

Austin Ladshaw: Methodology, Software, Validation, Investigation, Writing – Original Draft, Visualization, **Josh Pihl:** Conceptualization, Methodology, Investigation, Writing – Review & Editing, Visualization, Supervision, Project Administration, Funding Acquisition.

Declaration of Competing Interest

The authors declare that they have no known competing financial interests or personal relationships that could have appeared to influence the work reported in this paper.

Acknowledgements

This research was supported by the DOE Office of Energy Efficiency and Renewable Energy (EERE), Vehicle Technologies Office and used resources at the National Transportation Research Center, a DOE-EERE User Facility at Oak Ridge National Laboratory. We appreciate the guidance of Siddiq Khan, Ken Howden, and Gurpreet Singh at DOE VTO and helpful discussions with our colleagues at the ORNL NTRC. We also thank the editors and reviewers for their support and volunteered time.

We dedicate this manuscript to the memory of C. Stuart Daw, an outstanding researcher and mentor who led this work during its early stages.

Appendix A. Supporting information

Supplementary data associated with this article can be found in the online version at doi:10.1016/j.apcatb.2021.120898.

References

[1] C.R. Thomas, J.A. Pihl, M.J. Lance, T.J. Toops, J.E. Parks II, J. Lauterbach, Effects of four-mode hydrothermal aging on three-way catalysts for passive selective catalytic reduction to control emissions from lean-burn gasoline engine, Appl. Cat. B: Enviro 244 (2019) 284–294, https://doi.org/10.1016/j.apcatb.2018.11.051.

[2] W. Li, K.L. Perry, K. Narayanaswamy, C.H. Kim, P. Najt, Passive ammonia SCR system for lean-burn SIDI engines, SAE Int. J. Fuels Lubr. 3 (2010) 99–106, https://doi.org/10.4271/2010-01-0366.

[3] J. Wang, H. Zhao, G. Haller, Y. Li, Recent advances in the selective catalytic reduction of NOx with NH3 on Cu-Chabazite catalysts, Appl. Cat. B: Enviro 202 (2017) 346–354, https://doi.org/10.1016/j.apcatb.2016.09.024.

[4] J. Li, H. Chang, L. Ma, J. Hao, R.T. Yang, Low-temperature selective catalytic reduction of NOx with NH3 over metal oxide and zeolite catalysts – a review, Catal. Today 175 (2011) 147–156, https://doi.org/10.1016/j.cattod.2011.03.034.

[5] D. Jo, G.T. Park, T. Ryu, S.B. Hong, Economical synthesis of high-silica LTA zeolites: a step forward in developing a new commercial NH3-SCR catalyst, 221-219, Appl. Cat. B: Enviro 243 (2019) 212–219, https://doi.org/10.1016/j.apcatb.2018.10.042.

[6] L. Ma, Y. Cheng, G. Cavataio, R.W. McCabe, L. Fu, J. Li, Characterization of commercial Cu-SSZ-13 and Cu-SAPO-34 catalysts with hydrothermal treatment for NH3-SCR of NOx in diesel exhaust, Chem. Eng. J. 225 (2013) 323–330, https://doi.org/10.1016/j.cej.2013.03.078.

[7] R. Villamaina, S. Liu, I. Nova, E. Tronconi, M.P. Ruggeri, J. Collier, A. York, D. Thompsett, Speciation of Cu cations in Cu-CHA catalysts for NH3-SCR: Effects of SiO2/AlO3 ratio and Cu-loading investigated by transient response methods, ACS Catal. 9 (2019) 8916–8927, https://doi.org/10.1021/acscatal.9b02578.

[8] J. Cheng, S. Han, Q. Ye, S. Cheng, T. Kang, H. Dai, Effects of hydrothermal aging at high and low temperatures on the selective catalytic reduction of NOx with NH3 over Cu/SAPO-34, Res. Chem. Inter. 45 (2019) 2023–2044, https://doi.org/10.1016/j.apcatb.2014.10.020.

[9] C. Niu, X. Shi, F. Liu, K. Liu, L. Xie, Y. You, H. He, High hydrothermal stability of Cu-SAPO-34 catalysts for the NH3-SCR of NOx, Chem. Eng. J. 294 (2016) 254–263, https://doi.org/10.1016/j.cej.2016.02.086.

[10] D. Wang, L. Zhang, K. Kamasamudram, W.S. Epling, In Situ-DRIFTS study of selective catalytic reduction of NOx by NH3 over Cu-exchanged SAPO-34, ACS Catal. 3 (2013) 871–881, https://doi.org/10.1021/cs300843k.

[11] W.P. Partridge, S.Y. Joshi, J.A. Pihl, N.W. Currier, New operando method for quantifying the relative half-cycle rates of the NO SCR redox cycle over Cu-exchanged zeolites, Appl. Cat. B: Enviro 236 (2018) 195–204, https://doi.org/10.1016/j.apcatb.2018.04.071.

[12] T. Yu, T. Hao, D. Fan, J. Wang, M. Shen, W. Li, Recent NH3-SCR Mechanism Research over Cu/SAPO-34 Catalyst, J. Phy. Chem. C. 118 (2014) 6565–6575, https://doi.org/10.1021/jp4114199.

[13] A.R. Fahami, T. Günter, D.E. Doronkin, M. Casapu, D. Zengel, T.H. Vuong, M. Simon, F. Breher, A.V. Kucherov, A. Brücker, J.D. Grunwaldt, The dynamic nature of Cu sites in Cu-SSZ-13 and the origin of the seagull NOx conversion profile during NH3-SCR, React. Chem. Eng. 4 (2019) 1000–1018, https://doi.org/10.1039/C8RE00290H.

[14] W. Su, H. Chang, Y. Peng, C. Zhang, J. Li, Reaction pathway investigation on the selective catalytic reduction of NO with NH3 over Cu/SSZ-13 at low temperatures, Environ. Sci. Technol. 49 (2015) 467–473, https://doi.org/10.1021/es503430w.

[15] F. Gao, D. Mei, Y. Wang, J. Szanyi, C.H.F. Peden, Selective catalytic reduction over Cu/SSZ-13: Linking Homo- and Heterogeneous catalysis, JACS 139 (2017) 4935–4942, https://doi.org/10.1021/jacs.7b01128.

[16] J.H. Kwak, D. Tran, S.D. Burton, J. Szanyi, J.H. Lee, C.H.F. Peden, Effects of hydrothermal aging on NH3-SCR reaction over Cu/zeolites, J. Catal. 287 (2012) 203–209, https://doi.org/10.1016/j.jcat.2011.12.025.

[17] G. Busca, L. Lietti, G. Ramis, F. Berti, Chemical and mechanistic aspects of the selective catalytic reduction of NOx by ammonia over oxide catalysts: a review, Appl. Cat. B: Enviro. 18 (1998) 1–36, https://doi.org/10.1016/S0926-3373(98)00040-X.

[18] F. Gao, J. Szanyi, On the hydrothermal stability of Cu/SSZ-13 SCR catalysts, Appl. Cat. A: Gen. 560 (2018) 185–194, https://doi.org/10.1016/j.apcata.2018.04.040.

[19] P.S. Dhillon, M.P. Harold, D. Wang, A. Kumar, S.Y. Joshi, Enhanced transport in washcoated monoliths: Application to selective lean NOx reduction and ammonia oxidation, Chem. Eng. J. 377 (2019), 119734, https://doi.org/10.1016/j.cej.2018.08.120.

[20] Y. Wang, Z. Li, R. Fan, X. Guo, C. Zhang, Y. Wang, Z. Ding, R. Wang, W. Liu, Deactivation and Regeneration for the SO2-Poisoning of a Cu-SSZ-13 Catalyst in the NH3-SCR Reaction, Catalysis 9 (2019) 797, https://doi.org/10.3390/catal9100797.

[21] Y. Shan, Y. Sun, J. Du, Y. Zhang, X. Shi, Y. Yu, W. Shan, H. He, Hydrothermal aging alleviates the inhibition effects of NO2 on Cu-SSZ-13 for NH3-SCR, Appl. Cat. B: Enviro 275 (2020), 119105, https://doi.org/10.1016/j.apcatb.2020.119105.

[22] J.A. Pihl, R. Blint, C.S. Daw, 2015 CLEERS Industry Priorities Survey Final Report, February 2016 ⟨https://cleers.org/wp-content/uploads/2017/02/2015_CLEERS_Industry_Priorities-Survey_Final_Report.pdf⟩ (accessed March 16, 2020).

[23] I. Lezcano-Gonzalez, U. Deka, B. Arstad, A. Van Yperen-De Deyne, K. Hemelsoet, M. Waroquier, V. Van Speybroeck, B.M. Weckhuysen, A.M. Beale, Determining the storage, availability and reactivity of NH3 within Cu-Chabazite-based Ammonia selective catalytic reduction systems, Phys. Chem. Chem. Phys. 16 (2014) 1639–1650, https://doi.org/10.1039/C3CP54132K.

[24] California Air Resources Board, Heavy-Duty Engine and Vehicle Omnibus Regulation and Associated Amendments. ⟨https://ww2.arb.ca.gov/rulemaking/2020/hdomnibuslownox⟩, 2020. (accessed June 6th, 2021).

[25] J. Luo, K. Kamasamudram, N.W. Currier, A. Yezerets, NH3-TPD methodology for quantifying hydrothermal aging of Cu/SSZ-13 SCR catalysts, Chem. Eng. Sci. 190 (2018) 60–67, https://doi.org/10.1016/j.ces.2018.06.015.

[26] H. Jiang, B. Guan, H. Lin, Z. Huang, Cu/SSZ-13 zeolites prepared by in situ hydrothermal synthesis method as NH3-SCR catalysts: Influence of the Si/Al ratio on the activity and hydrothermal properties, Fuel 255 (2019), 115587, https://doi.org/10.1016/j.fuel.2019.05.170.

[27] F. Gao, N.M. Washton, Y. Wang, M. Kollár, J. Szanyi, C.H.F. Peden, Effects of Si/Al ratio on Cu/SSZ-13 NH3-SCR catalysis: Implications for active Cu species and the rotes of Brønsted acidity, J. Catal. 331 (2015) 25–38, https://doi.org/10.1016/j.jcat.2015.08.004.

[28] W. Hu, T. Selleri, F. Gramigni, E. Fenes, K.R. Rout, S. Liu, I. Nova, D. Chen, X. Gao, E. Tronconi, On the Redox Mechanism of Low-Temperature NH3-SCR over Cu-CHA: A Combined Experimental and Theoretical Study of the Reduction Half Cycle, Angew. Chem. Int. Ed. 60 (2021) 7197–7204, https://doi.org/10.1002/anie.202014926.

[29] X. Auvray, O. Mihai, B. Lundberg, L. Olsson, Deactivation of Cu/SSZ-13 NH3-SCR Catalyst by Exposure to CO, H2, and C3H6, Catalysis 9 (2019) 929, https://doi.org/10.3390/catal9110929.

[30] L. Chen, T.V.W. Janssens, M. Skoglundh, H. Grönbeck, Interpretation of NH3-TPD profiles from Cu-CHA using first-principles calculations, Top. Catal. 62 (2019) 93–99, https://doi.org/10.1007/s11244-018-1095-y.
[31] E. Borfecchia, C. Negri, K.A. Lomachenko, C. Lamberti, T.V.W. Janssens, G. Berlier, Temperature-dependent dynamics of NH3-derived Cu species in the Cu-CHA SCR catalyst, React. Chem. Eng. 4 (2019) 1067–1080, https://doi.org/10.1039/c8re00322j.
[32] R. Daya, S.Y. Joshi, J. Luo, R.K. Dadi, N.W. Currier, A. Yezerets, On kinetic modeling of change in active sites upon hydrothermal aging of Cu-SSZ-13, Appl. Cat. B: Enviro 263 (2020) 118368–118379, https://doi.org/10.1016/j.apcatb.2019.118368.
[33] L. Olsson, K. Wijayanti, K. Leistner, A. Kumar, S.Y. Joshi, K. Kamasamudram, N. W. Currier, A. Yezerets, A multi-site kinetic model for NH3-SCR over Cu/SSZ-13, Appl. Cat. B: Enviro 174 (2015) 212–224, https://doi.org/10.1016/j.apcatb.2015.02.037.
[34] L. Olsson, K. Wijayanti, K. Leistner, A. Kumar, S.Y. Joshi, K. Kamasamudram, N. W. Currier, A. Yezerets, A kinetic model for sulfur poisoning and regeneration of Cu/SSZ-13 used for NH3-SCR, Appl. Cat. B: Enviro. 184 (2016) 394–406, https://doi.org/10.1016/j.apcatb.2015.11.001.
[35] Z. Gao, J. Pihl, T. LaClair, B. Fricke, Global kinetic modeling of NH3-SCR with two sites of NH3 storage on Cu-SSZ-13, Chem. Eng. J. 406 (2021), 127120, https://doi.org/10.1016/j.cej.2020.127120.
[36] S. Sinha Majumdar, J.A. Pihl, T.J. Toops, Reactivity of novel high-performance fuels on commercial three-way catalysts for control of emissions from spark-ignition engines, Appl. Energy 255 (2019) 294–304, https://doi.org/10.1016/j.apenergy.2019.113640.
[37] M. Colombo, I. Nova, E. Tronconi, Detailed kinetic modeling of the NH3–NO/NO2 SCR reactions over a commercial Cu-zeolite catalyst for Diesel exhausts after treatment, Catal. Today 175 (2012) 243–255, https://doi.org/10.1016/j.cattod.2012.09.002.
[38] K. Xie, A. Wang, J. Woo, A. Kumar, K. Kamasamudram, L. Olsson, Deactivation of Cu-SSZ-13 SCR catalysts by vapor-phase phosphorus exposure, Appl. Cat. B: Enviro 256 (2019), 117815, https://doi.org/10.1016/j.apcatb.2019.117815.
[39] C. Paolucci, A.A. Verma, S.A. Bates, V.F. Kispersky, J.T. Miller, R. Gounder, W. N. Delgass, F.H. Ribeiro, W.F. Schneider, Isolation of the copper redox steps in the standard selective catalytic reduction on Cu-SSZ-13, Angew. Chem. Int. Ed. 53 (2014) 11828–11833, https://doi.org/10.1002/anie.201407030.
[40] C. Paolucci, A.A. Parekh, I. Khurana, J.R. Di Iorio, H. Li, J.D.A. Caballero, A. J. Shih, T. Anggara, W.N. Delgass, J.T. Miller, F.H. Ribeiro, R. Gounder, W. F. Schneider, Catalysis in a cage: condition-dependent speciation and dynamics of exchanged Cu cations in SSZ-13 zeolites, JACS 138 (2016) 6028–6048, https://doi.org/10.1021/jacs.6b02651.
[41] H. Lee, I. Song, S.W. Jeon, D.H. Kim, Inter-particle migration of Cu ions in physically mixed Cu-SSZ-13 and H-SSZ-13 treated by hydrothermal aging, React. Chem. Eng. 4 (2019) 1059–1066, https://doi.org/10.1039/C8RE00281A.
[42] T.V.W. Janssens, H. Falsig, L.F. Lundegaard, P.N.R. Vennestrøm, S.B. Rasmussen, P. G. Moses, F. Giordanino, E. Borfecchia, K.A. Lomachenko, C. Lamberti, S. Bordiga, A. Godiksen, S. Mossin, P. Beato, A consistent reaction scheme for the selective catalytic reduction of nitrogen oxides with ammonia, ACS Catal. 5 (2015) 2832–2845, https://doi.org/10.1021/cs501673g.
[43] C. Tien, Adsorption Calculations and Modeling, Newton, Massachusetts, 1994.
[44] I. Nova, D. Bounechada, R. Maestri, E. Tronconi, A.K. Heibel, T.A. Collins, T. Boger, Influence of the Substrate Properties on the Performance of NH3-SCR Monolithic Catalysts for the Aftertreatment of Diesel Exhaust: An Experimental and Modeling Study, Ind. Eng. Chem. Res. 50 (2011) 299–309, https://doi.org/10.1021/ie1015409.
[45] Y. Kim, T. Park, C. Jung, C.H. Kim, Y.W. Kim, J.M. Lee, Hybrid Nonlinear Model Predictive Control of LNT and Urealess SCR Aftertreatment System, IEEE Trans. Con. Sys. Tech. 27 (2019) 2305–2313, https://doi.org/10.1109/TCST.2018.2857722.
[46] A. Ladshaw, L.J. Kuo, J. Strivens, J. Wood, N. Schlafer, S. Yiacoumi, C. Tsouris, G. Gill, Influence of Current Velocity on Uranium Adsorption from Seawater Using an Amidoxime-Based Polymer Fiber Adsorbent, Ind. Eng. Chem. Res. 56 (2017) 2205–2211, https://doi.org/10.1021/acs.iecr.6b04539.
[47] A. Ladshaw, A.I. Wiechert, A.K. Welty, K.L. Lyon, J.D. Law, R.T. Jubin, C. Tsouris, S. Yiacoumi, Adsorbents and adsorption models for capture of Kr and Xe gas mixtures in fixed-bed columns, Chem. Eng. J. 375 (2019), 122073, https://doi.org/10.1016/j.cej.2019.122073.
[48] M.E. Davis, R.J. Davis, Fundamentals of Chemical Reaction Engineering, N. Y., N. Y. (2003).
[49] C.J. Permann, D.R. Gaston, D. Andrš, R.W. Carlsen, F. Kong, A.D. Lindsay, J. M. Miller, J.W. Peterson, A.E. Slaughter, R.H. Stogner, R.C. Martineau, MOOSE: Enabling massively parallel multiphysics simulation, SoftwareX 11 (2020), 100430, https://doi.org/10.1016/j.softx.2020.100430.
[50] B. Rivière, Discontinuous Galerkin Methods for Solving Elliptic and Parabolic Equations: Theory and Implementation, SIAM,, Philadelphia, 2008, https://doi.org/10.1137/1.9780898717440.
[51] D.A. Knoll, D.E. Keyes, Jacobian-Free Newton-Krylov methods: a survey of approaches and applications, J. Comp. Phys. 193 (2004) 357–397, https://doi.org/10.1016/j.jcp.2003.08.010.
[52] A. Ladshaw, CATS: Catalytic After Treatment System, ⟨https://github.com/aladshaw3/cats⟩ (accessed 1 June 2021).
[53] J.R.D. Iorio, S.A. Bates, A.A. Verma, W.N. Delgass, F.H. Ribeiro, J.T. Miller, R. Gounder, The Dynamic Nature of Brønsted Acid Sites in Cu–Zeolites During NOx Selective Catalytic Reduction: Quantification by Gas-Phase Ammonia Titration, Top. Catal. 58 (2015) 424–434, https://doi.org/10.1007/s11244-015-0387-8.
[54] X. Li, Y. Zhao, H. Zhao, M. Liu, Y. Ma, X. Yong, H. Chen, Y. Li, The Cu migration of Cu-SAPO-34 catalyst for ammonia selective catalytic reduction of NOx during high temperature hydrothermal aging treatment, Catal. Today 327 (2019) 126–133, https://doi.org/10.1016/j.cattod.2018.05.029.
[55] K. Supriyanto, K. Wijayanti, A. Kumar, S.Y. Joshi, K. Kamasamudram, N. W. Currier, A. Yezerets, L. Olsson, Global kinetic modeling of hydrothermal aging of NH3-SCR over Cu-zeolites, Appl. Cat. B: Enviro 163 (2015) 382–392, https://doi.org/10.1016/j.apcatb.2014.07.059.